New developments in the design of welded or bolted single steel angle members in compression

Markus Kettler[1], Paul Zauchner[2], Harald Unterweger[3]

Abstract
The practical design of single steel angle members in compression has to cover multiple effects. Due to the commonly eccentric connection on only one angle leg (bolted or welded), additional bending moments are acting on the member, leading to a complex load carrying behavior with flexural and/or lateral torsional buckling phenomena. Furthermore, type and size of rotational restraints at the member's ends (provided by the adjacent structure) significantly influence the compression member capacity of these members.

Within this paper, a recently developed design approach for angle members in compression is introduced. The presented method allows for calculating the internal forces based on elastic second order theory for an individual member with eccentricities and rotational spring stiffness at both ends. This calculation can be carried out by means of conventional structural analysis software. Detailed analytical models for the estimation of appropriate spring stiffness values for several practical applications in buildings with two-bolt connections have recently been presented by the authors. The proposed design method is now enhanced by means of additional formulae for angle members welded to the adjacent structure. Detailed background information on the derivation of these newly developed spring stiffness formulae is given. Finally, the accuracy of the design model for this enlarged range of application for welded angle members is shown through comparison with sophisticated finite element calculations, code provisions (AISC 360 and EN 1993-1-1) and experimental tests from literature.

1. Introduction
Single steel angle struts are frequently used as bracing members in buildings. At their ends, they are commonly bolted or welded to the adjacent structure by only one angle leg. This eccentric load introduction leads to additional bending moments in the member, resulting in a complex load carrying behavior with flexural and/or lateral torsional buckling phenomena. In addition, the bolted or welded connections provide rotational restraints at the member's ends, which significantly influence the compression member capacity of these angle struts.

---
[1] Associate Professor, Graz University of Technology – Austria, <kettler@TUGraz.at>
[2] Graduate Research Assistant, Graz University of Technology – Austria, < p.zauchner@tugraz.at >
[3] Professor, Graz University of Technology – Austria, < h.unterweger@TUGraz.at>

Several experimental tests on single steel angles in compression with eccentric load introduction through only one angle leg were conducted in the past. The focus of the following short literature review is on equal-leg hot-rolled angle sections with one angle leg welded to the adjacent structure. A comprehensive comparison of cases with bolted angle sections is given in Kettler et al. 2017.

Trahair et al. 1969 conducted an experimental testing campaign that systematically investigated the influence of support conditions on the load carrying behaviour of eccentrically loaded single angles. 34 tests were carried out on equal-leg angle sections with the following dimensions: 2 in. x 2 in. x ¼ in. (b = 50.8 mm, t = 6.35 mm). They were welded by one leg to structural tee stubs (web thickness = 10.9 mm) and were tested with different boundary conditions (i.e. fixed-end or knife-edge support conditions). The test results for BC1 (rigid support, 15 tests) and BC2 (knife-edge support, 11 tests) are plotted in Fig. 1 and are compared to current design standards. In section 4 of this paper, the test results are also compared to the new design proposal.

Sakla 1997 reported on 51 compression tests on single angle members welded by one leg to webs of tee sections. The cross-section of the angle struts was of type L 64x64x7.9 mm. The web thickness of the tee sections was varied between 10.2 and 12.7 mm. The 39 tests with equal weld pattern are used for comparison within this paper.

Schneider 2003 presented 13 tests on hot-rolled single steel angles welded to gusset plates. The gusset plate thickness was varied between 15 and 25 mm. Angle sections with the following dimensions were tested: L 80x80x8, L 120x120x12 and L 120x80x12 (dimensions in mm). The 6 tests with equal-leg angle sections are considered within this paper.

2. Comparison of test results with current design standards
Fig. 1 shows a comparison of the mentioned experimental test results from literature with the design rules of AISC 360 and EN 1993-1-1 (see CEN 2014).
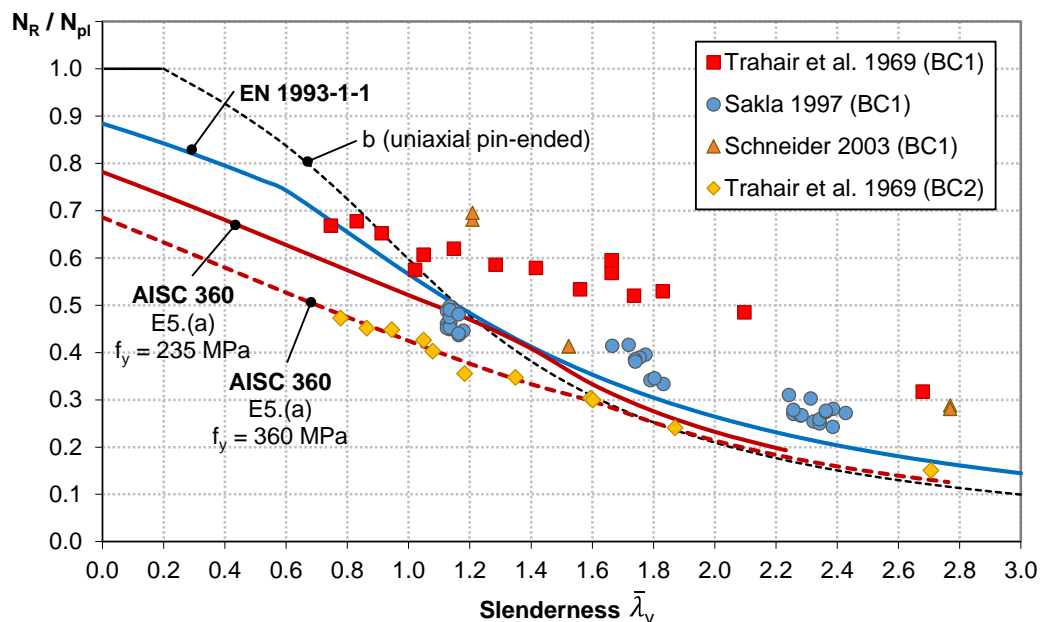

Figure 1: Comparison of experimental test results with current design specifications
(BC1= rigid support, BC2 = knife edge support).

2

The ultimate loads of the tests $N_{R,test}$ are related to the plastic resistance to axial force of the gross cross-section N_{pl} and are plotted over the non-dimensional slenderness of the angle sections about the minor axis $\bar{\lambda}_v$, based on the system length L. For this purpose, $N_{pl} = A \cdot f_y$, where A is the cross-sectional area and f_y is the yield strength. The code resistance curves were also plotted over $\bar{\lambda}_v$. This was realized by assuming the ratio of the radius of gyration about the axis parallel to the outstanding angle leg i_y and about the minor axis i_v being $i_y/i_v = 1.56$. This value was found to be an excellent approximation for the product range of European hot rolled equal-leg angle sections. It can be verified from Fig. 1 that the capacities of EN 1993-1-1 result in a single resistance curve, while the capacities of AISC 360 depend on the yield strength. For the latter, two curves are plotted. The chosen yield strengths are $f_y = 235$ N/mm² and $f_y = 360$ N/mm². Comparing the test results for fixed-ended boundary conditions BC1 with the Eurocode resistances illustrates quite good accordance for the tests from Sakla 1997, but reveals significant underestimation of the real capacity for the tests from Trahair 1969. The capacities of AISC 360 are considerably smaller than the ultimate loads of the two testing campaigns. The limited number of available tests from Schneider 2003 does not allow for profound conclusions, but the test ultimate loads are all larger than the code predictions.

It can clearly be verified from Fig. 1 that the boundary conditions (i.e. the rotational restraints at the members ends) have a significant influence on the compression member capacity of welded angle struts. Based on numerical results in Kettler et al. 2017 and additional experimental tests in Kettler et al. 2019, the authors illustrated a similar behaviour for angle columns bolted to gusset plates. Therefore, detailed analytical models for the estimation of appropriate rotational spring stiffness values for several typical bolted end connections were developed in Kettler et al. 2019a. These results provided the basis for a design proposal for bolted angle struts that was presented in Kettler et al. 2021. The proposed design method is enhanced by means of additional formulae for angle members welded to the adjacent structure within this paper.

3. Design proposal for welded angle struts
Fig. 2 presents the details of the proposed design procedure with welded connections on both members ends.
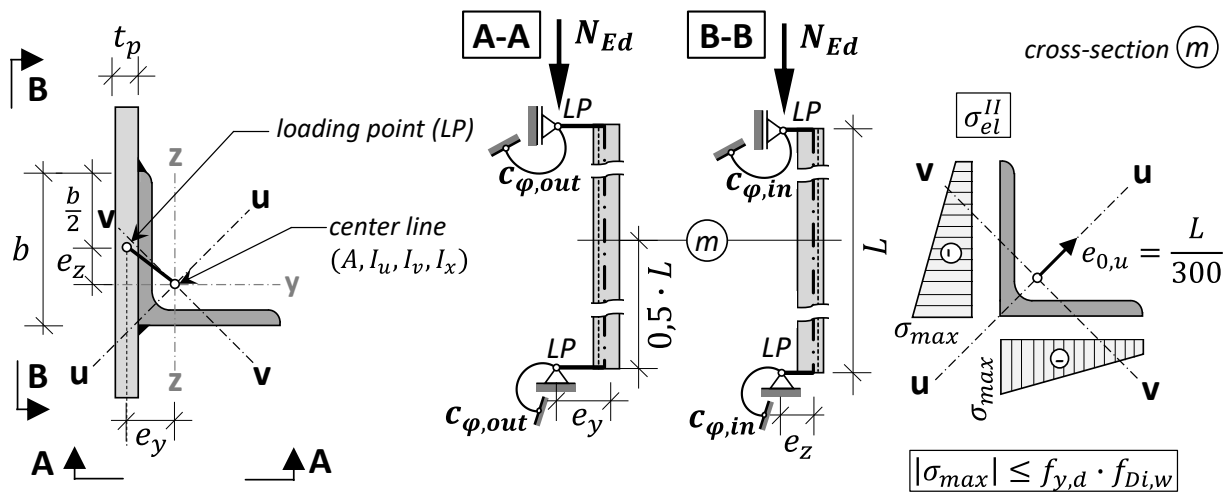

Figure 2: Design model for welded angle struts.

3

The design model is based on a 3D-beam model with bending stiffness about main axes u and v and torsional stiffness as well as eccentricities (e_y, e_z) and rotational spring stiffness ($c_{\varphi,in}$, $c_{\varphi,out}$) at both ends. The loading point is assumed centric between the two longitudinal welds in the mid-plane of the gusset plate or at the top of the adjacent girder flange, respectively. The calculation of the internal forces based on second order theory should preferably be carried out by means of a conventional structural analysis software. An equivalent bow imperfection, with amplitude $e_{0,u} = L/300$ about the minimum axis should be taken into account. The design check is fulfilled, if the maximum direct stresses in the angle member due to the acting axial force N_{Ed} (which is the result of a previous global analysis of the steel structure, where the eccentricity of the angle member and the joint stiffness may be neglected) are not larger than the design yield strength $f_{y,d}$ multiplied with a factor $f_{Di,w}$, based on model calibration, see Eq. (1).

$$|\sigma_{max}| \leq f_{y,d} \cdot f_{Di,w} \tag{1}$$

The design model allows the simplest application in practice, with verification whether the design axial force N_{Ed} in the angle is acceptable or not. The typically higher ultimate capacity $N_{R,model}$ can be calculated, if needed, by increasing the external load N_{Ed} until the maximum direct stresses in the member reach the design yield stress $f_{y,d}$. The thereby calculated resistance force $N_{R,1D}$ is then multiplied with the calibration factor $f_{Di,w}$ to reach the compression member capacity $N_{R,model} = N_{R,1D} \cdot f_{Di,w}$.

One of the most crucial parameters are the rotational end restraints $c_{\varphi,in}$ and $c_{\varphi,out}$, which mainly depend on the adjacent structure. Analytical formulae have been developed for several practical applications. The corresponding equations are presented in Eqs. (5) and (6) and in Fig. 6. The investigated joint configurations with welded connections are illustrated in Fig. 3.
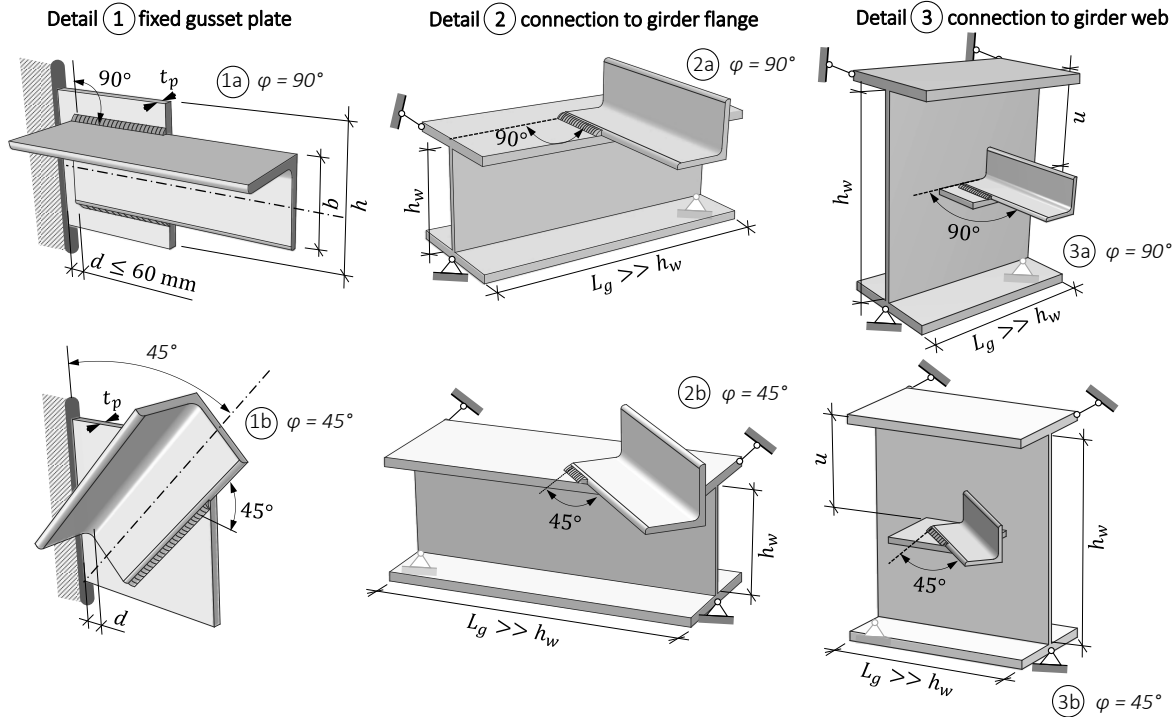

Figure 3: Investigated joint types that are covered by the new design model.
(Note for detail 3: $0 < u/h_w < 1.0$)

4

Detail 1 is a simple welded gusset plate connection to a fixed support (comparable to BC1 of the laboratory tests). In detail 2 the angle section is welded to the upper flange of an I-shaped girder of length L_g. Detail 3 consists of a welded gusset plate connection to the web of an I-shaped girder. The girder length L_g also reflects the distances of flange supports out of plane. The appropriate end restraints $c_{\varphi,in}$ and $c_{\varphi,out}$ provided by these joint types (in and out of plane of the gusset plate, or the upper flange of the girder, respectively) can be calculated with the formulae presented in Eq. (5) and (6) as well as in Fig. 6.

The calibration factors $f_{Di,w}$ for the investigated welded joint types detail 1 to detail 3 are given in Eqs. (2) to (4). They are covering the effects of the following two simplifications of the design model: (i) the rotational stiffness coefficients $c_{\varphi,in}$ and $c_{\varphi,out}$ are based on elastic theory. Potential stiffness reduction due to local plastification in the region of the connection should be covered by $f_{Di,w}$. (ii) the beam model assumes a constant bending stiffness along the whole member length L (see Fig. 2) equal to the angle's geometric properties. The fact that this stiffness parameter in reality changes in the region of the connections (e.g. gusset plate plus angle) should also be covered by $f_{Di,w}$. These two effects generally lead to a resistance reduction for slender members and to an increase in capacity for shorter members. The calibration of the $f_{Di,w}$ factors was conducted based on a finite element parametric study and was part of the validation process of the design model, see section 4. In this respect it is noted that the proposed calibration factors for welded connections in Eqs. (2) to (4) are not identical with the corresponding factors in Kettler et al. 2021 for bolted connections. This can be explained by the slightly different deformation behaviour of welded and bolted connections.

Detail 1: fixed gusset plate (both types 1a and 1b)
$$f_{D1,w} = 1.25 - 0.28 \cdot \bar{\lambda}_v + 0.04\bar{\lambda}_v^2 \leq 1.09 \tag{2}$$

Detail 2: connection to girder flange (both types 2a and 2b)
$$f_{D2,w} = 1.51 - 0.3 \cdot \bar{\lambda}_v + 0.045\bar{\lambda}_v^2 \leq 1.3 \tag{3}$$

Detail 3: connection to girder web (both types 3a and 3b)
$$f_{D3,w} = 1.35 - 0.2 \cdot \bar{\lambda}_v + 0.02\bar{\lambda}_v^2 \leq 1.2 \tag{4}$$

Although bolted connections with at least two bolts in the connected leg provide approximately the same rotational restraints as their welded counterparts, the local deformations and stresses in the region of the connections are significantly different. For that reason, new formulae for the rotational out of plane restraints of welded gusset plate connections (detail 1) have been developed. Fig. 4 presents the investigated configurations including geometric parameters. Detail 1a shows a member axis perpendicular to the support and detail 1b shows an inclination of 45°. The figure also illustrates the moment distribution out of plane of the gusset plate within the theoretical model of a cantilever beam, that is the basis for determination of the rotational stiffness $c_{\varphi l,out}$. The cantilever (i.e. the gusset plate) is loaded by a single load at the end of the angle section and by an additional constant line load in opposite direction, representing the punctual compression of the angle section and the continuous tension of the weld, respectively. This results in a moment distribution with a constant and a parabolic part. These moment distributions have been validated with a numerical parametric study, using finite element models with solid elements.
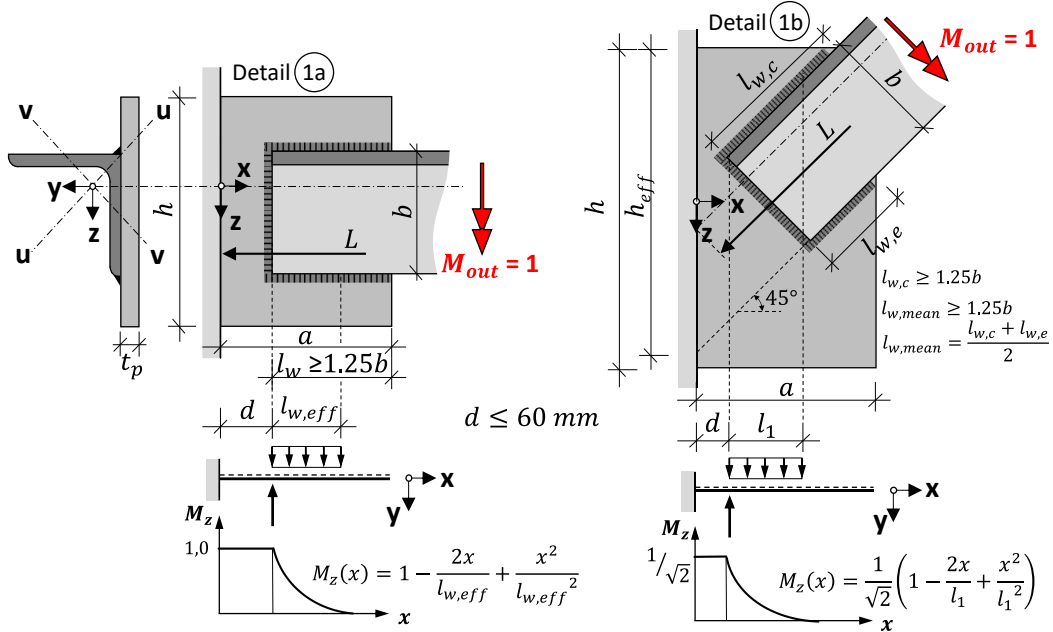
Figure 4: Determination of moment distribution in simplified beam model of detail 1 for the calculation of $c_{\varphi1,out}$.

Eq. (5) shows the derivation of the rotational stiffness $c_{\varphi1a,out}$ for detail 1a:

$$c_{\varphi1a,out} = \frac{M_{out}}{\varphi} = \frac{1}{\varphi} = \frac{EI}{\int M_z \cdot \bar{M}_z \cdot dx} = \frac{5 \cdot EI}{5d + l_{w,eff}} = \frac{5E \cdot h_{eff} t_p^3}{12(5d + l_{w,eff})} \tag{5}$$

where E is the modulus of elasticity, t_p is the thickness of the gusset plate, d is defined in Fig. 4, $h_{eff} = 2l_w + 4d$, l_w is the weld length and $l_{w,eff} = \frac{h_{eff} + d}{4}$.

The same procedure is applied to detail 1b, resulting in the following stiffness function:

$$c_{\varphi1b,out} = \sqrt{2} \frac{5 \cdot EI}{5d + l_1} = \frac{5\sqrt{2} \cdot E \cdot h_{eff} t_p^3}{12(5d + l_1)} \tag{6}$$

where d is defined in Fig. 4, $h_{eff} = \frac{l_{w,mean}}{\sqrt{2}} + b\sqrt{2} + d \leq h$

and $l_1 = \frac{h_{eff} + d}{4} \cdot \frac{t_p}{t_{p,min}} \leq min\left(b; \frac{l_{w,mean}}{\sqrt{2}}\right)$ with $t_{p,min} = 10\ mm$.

Fig. 5 presents a comparison of some of the results of the conducted numerical parametric study with the proposed analytic formulae for details 1a and 1b. Dashed lines thereby indicate the analytic stiffness functions. The finite element calculations were carried out for the equal leg angle section L80x8 with elastic material behaviour ($E = 210\ 000$ N/mm²) for the gusset plates. The short angle section was assumed as rigid in order to simplify the determination of the end rotation φ. The deformation of the angle section itself will subsequently be accounted for in the design model (see Fig. 2). Therefore, the assumption of a rigid angle for the herein presented numerical calculations, avoids considering the angle deformations twice. A single moment M_{out} was applied at the end of the angle section. The rotational stiffness of the investigated detail was then calculated

6

by dividing the applied moment M by the resulting rotation φ of the FE-calculations, based on Eq. (6).
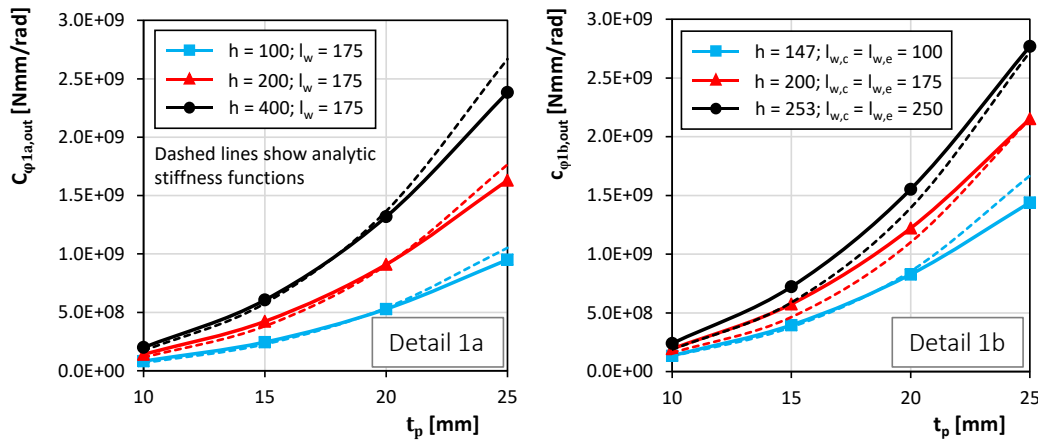

Figure 5: Comparison of numerical parametric study (FEM) with proposed analytic formulae for details 1a and 1b with varying gusset plate thickness t_p and $d = 20$ mm.

The comparison in Fig. 5 indicates that the proposed stiffness functions for detail 1 are in good accordance with the finite element results. Only for some cases, small differences are visible, which have a negligible influence on the ultimate capacity of the angle struts. Therefore, it is concluded that the proposed stiffness functions in Eqs. (5) and (6) can appropriately describe the real out of plane rotational behaviour of detail 1. The rotational stiffness in plane of the gusset plate can be assumed as infinite for detail 1a and detail 1b ($c_{\varphi 1,in} = \infty$).

Fig. 6 presents the proposed stiffness functions $c_{\varphi,in}$ and $c_{\varphi,out}$ for the welded details 2 and 3. It was found that the stiffness behaviour of welded and bolted connections is very similar for these two configurations. Generally, it is the flexibility of the girder's web (and not the bolted or welded connection itself) that governs the overall stiffness. Therefore, the presented formulae are analogous to the formulae for bolted connections, published in Kettler et al. 2021. The accurate length L of the angle member for the design procedure (i.e. the beam model) is also identified in the illustrations of the individual joint types in Fig. 6 as well as in Fig. 4.

The following criteria further specify the area of application of the proposed design model:
- The length of the longitudinal welds should meet the following criteria for all joint details: $l_w \geq 1.25 \cdot b$
- The model is calibrated for equal-leg angle members. It is assumed that the new model is also safe for unequal angle members, where the longer angle leg is welded to the adjacent structure. However, this is not yet validated by experimental tests or FE calculations.
- Local buckling of the angle member is not included in the design model. Therefore, at least a class 3 section, based on EN 1993-1-1, is required.
- The geometric minimum and maximum values of Fig. 4 should be considered and the minimum thickness of the gusset plate is suggested with $t_{p,min} = 10$ mm.
- The free length of the gusset plate d should be less than or equal to 60 mm for details 1 and 3.

- The range of application of the proposed design model is given by $0.5 \leq \bar{\lambda}_v \leq 2.8$. If $\bar{\lambda}_v < \bar{\lambda}_{v,min} = 0.5$, the member capacity should be calculated with $\bar{\lambda}_{v,min}$ and the corresponding minimum member length L_{min} based on Eq. (7).

$$L_{min} = 0.50 \cdot i_v \cdot \lambda_1 = 46.95 \cdot i_v \cdot \sqrt{\frac{235}{f_y}} \tag{7}$$

The upper slenderness limit of 2.8 was chosen based on the available experimental tests and the parameter range of the conducted numerical calculations.
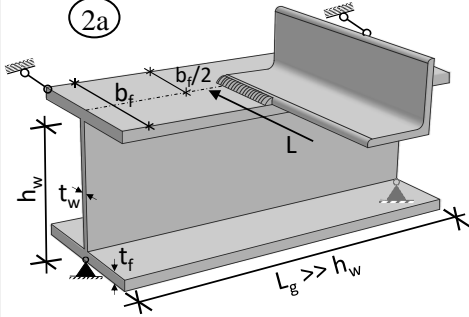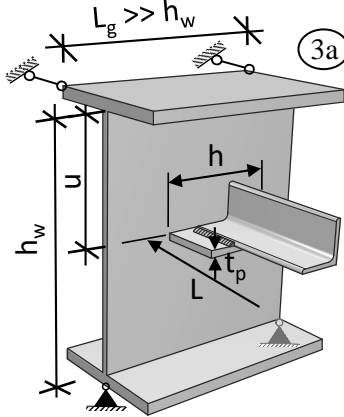
Detail		$c_{\varphi i,in}$		
		$c_{\varphi i,out}$		
2a and 2b	②a	$c_{\varphi 2,in} = \infty$		
		$c_{\varphi 2,out,loc} = $ $= \dfrac{0.45 \cdot E \cdot t_w^{1.75} \cdot t_f^{1.25} \cdot b_f^{0.5}}{h_w^{0.5}}$ $c_{\varphi 2,out,glob} = \dfrac{4 \cdot E \cdot h_w^2 \cdot t_f \cdot b_f^3}{L_g^3}$	$c_{\varphi 2,out} = $ $= \dfrac{1}{\dfrac{1}{c_{\varphi 2,out,loc}} + \dfrac{1}{c_{\varphi 2,out,glob}}}$ ②a $c_{\varphi 2b,out} = 2 \cdot c_{\varphi 2,out}$ ②b	
3a and 3b	③a	$c_{\varphi 3,in,loc} = \dfrac{K \cdot \pi^3 \cdot h}{h_w \cdot sin^2\left(\dfrac{\pi \cdot u}{h_w}\right)}$ $c_{\varphi 3,in,glob} = \dfrac{12 \cdot EI_z}{L_g}$	$c_{\varphi 3,in} = $ $= \dfrac{1}{\dfrac{1}{c_{\varphi 3,in,loc}} + \dfrac{1}{c_{\varphi 3,in,glob}}}$ ③a = ③b	
		$c_{\varphi 3,out,web} = \dfrac{70 \cdot E \cdot t_w^{1.6}}{h_w^{0.25}} \cdot K_{web}$ $c_{\varphi 3,out,glob} = $ $= \dfrac{1}{\dfrac{L_g}{4 \cdot GI_T} \cdot \left(1 - \dfrac{\tanh \varepsilon_T}{\varepsilon_T}\right)}$	$c_{\varphi 3,out} = $ $= \dfrac{1}{\dfrac{1}{c_{\varphi 1a,out}} + \dfrac{1}{c_{\varphi 3,out,glob}} + \dfrac{1}{c_{\varphi 3,out,web}}}$ ③a $c_{\varphi 3,out}$ with $c_{\varphi 1b,out}$ and $c_{\varphi 3b,out,glob} = 2.5 \cdot c_{\varphi 3,out,glob}$ $c_{\varphi 3b,out,web} = 2.5 \cdot c_{\varphi 3,out,web}$ ③b	
Parameters:	$\varepsilon_T = \sqrt{\dfrac{I_T}{2.6 \cdot I_\omega}} \cdot \dfrac{L_g}{2}$	$K = \dfrac{E \cdot t_w^3}{12 \cdot (1 - v^2)}$	$K_{web} = \dfrac{1}{4 \cdot \left(1 - 3\dfrac{u}{h_w} + 3\left(\dfrac{u}{h_w}\right)^2\right)}$	
where:	L_g girder length $\quad$ G shear modulus	I_T, I_ω, I_z torsional, warping and bending stiffness of girder $\quad$ v Poisson´s ratio for steel (v = 0.3)		

Figure 6: Stiffness functions $c_{\varphi,in}$ and $c_{\varphi,out}$ for details 2 and 3.

4. Validation of design model

In order to validate the proposed design model, the predicted capacities are compared to available test results from literature and to the results of an additional numerical parametric study also presented in this section.

Fig. 7 shows a comparison of the design model and the provisions of AISC 360 and EN 1993-1-1 with the tests from Trahair et al. 1969, Sakla 1997 and Schneider 2003 with boundary condition BC1 (i.e. detail 1a). In total, 60 tests are considered. The ultimate loads from the tests $N_{R,test}$ are referred to the predicted capacities N_R and plotted over the non-dimensional slenderness $\bar{\lambda}_v$ about the weak axis. The comparison is done on basis of measured yield strength f_y and measured Young's modulus E without any safety factors. In addition to the data points, linear regression lines are presented for the results of AISC 360 and EN 1993-1-1. The results indicate that both code provisions can lead to significant uneconomic predictions of the real compression capacities. EN 1993-1-1 shows unsafe results for 16 out of 60 investigated tests. AISC 360 is conservative for all cases, but underestimates the capacities in 8 cases by a factor two or more. In contrast to that, the results of the proposed design model show good accordance with the test results. On average, the capacities of the compression tests are 19% higher than the predicted resistances.
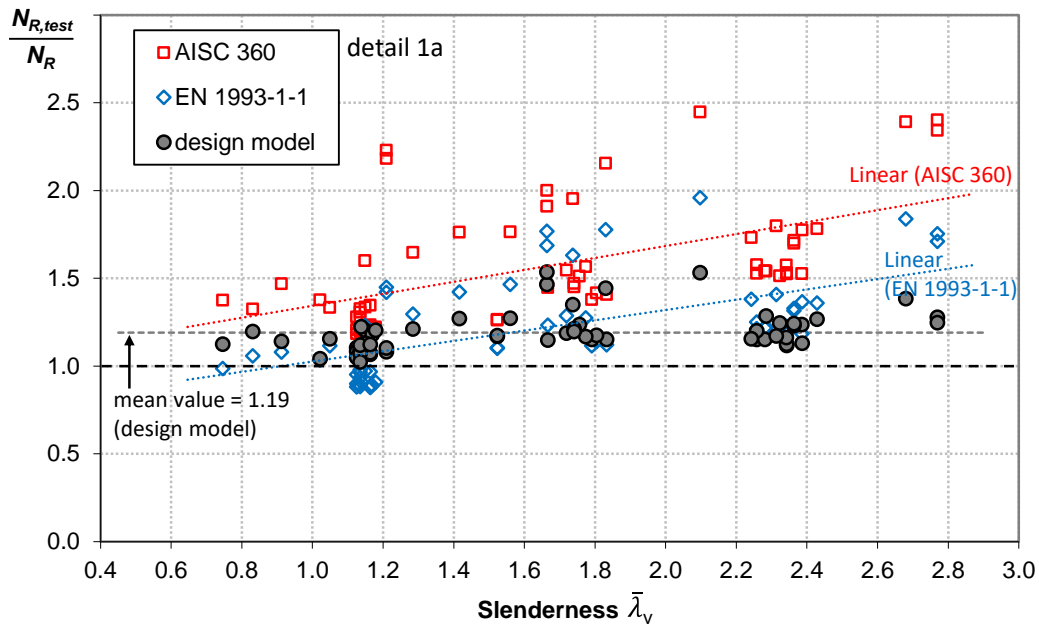
Figure 7: Comparison of test results with BC1 to compressive strength according to AISC 360, EN 1993-1-1 and the proposed design model for detail 1a.

Table 1 summarizes the comparison of results for the investigated laboratory tests. The stiffness function $c_{\varphi,out}$ corresponds to $c_{\varphi1a,out}$ in Eq. (6) for detail 1a. The rotational stiffness in plane of the gusset plate is infinite ($c_{\varphi,in} = \infty$). The calibration factor f_{Di} corresponds to $f_{D1,w}$ in Eq. (2) for detail 1a. The statistical parameters at the end of Table 1 confirm the accuracy of the proposed design model and the improvement compared to the existing code procedures.

Table 1: Comparison of design proposal with tests from literature for detail 1a (BC1)

$\bar{\lambda}_v$ [-]	t_p [mm]	$N_{R,test}$ [kN]	N_{pl}[1] [kN]	$c_{\varphi,out}$[2] $[\frac{kNm}{rad}]$	$f_{D1,w}$ [-]	$N_{R,model}$ [kN]	$\frac{N_{R,test}}{N_{R,model}}$	$\frac{N_{R,test}}{N_{R,AISC}}$[3]	$\frac{N_{R,test}}{N_{R,EC}}$[4]
Trahair et al. 1969, L50.8/6.4									
A-1-1	2.68	10.9	68	214	153	0.79	49.2	1.38	2.39	1.84
A-1-2	2.10	10.9	103	212	153	0.84	67.3	1.53	2.45	1.96
A-1-3	1.83	10.9	113	213	153	0.87	78.4	1.44	2.15	1.78
A-1-4	1.74	10.9	111	213	153	0.88	82.2	1.35	1.95	1.63
A-1-5	1.56	10.9	115	216	153	0.91	90.4	1.27	1.76	1.46
A-1-6	1.42	10.9	123	212	153	0.93	96.8	1.27	1.76	1.42
A-1-7	1.28	10.9	125	213	153	0.96	103.3	1.21	1.65	1.29
A-1-8	1.15	10.9	132	213	153	0.98	109.7	1.20	1.60	1.23
A-1-9	1.02	10.9	121	211	153	1.01	116.3	1.04	1.38	1.03
A-1-10	0.91	10.9	138	212	153	1.03	121.0	1.14	1.47	1.08
A-1-11	0.75	10.9	140	209	153	1.05	124.5	1.12	1.37	0.98
B-1-1	1.66	10.9	105	185	153	0.89	71.7	1.46	1.91	1.69
B-1-1a	1.66	10.9	110	185	153	0.89	71.7	1.53	2.00	1.77
B-1-5	1.05	10.9	112	185	153	1.00	97.0	1.15	1.33	1.11
B-1-6	0.83	10.9	125	185	153	1.05	104.5	1.20	1.32	1.06
Sakla 1997, L64/7.9									
L-A-1	2.26	10.2	89.3	330	103	0.82	77.7	1.15	1.53	1.21
L-A-2	2.28	10.2	90.1	337	103	0.82	78.3	1.15	1.54	1.22
L-A-3	2.34	10.2	89.5	356	103	0.81	80.1	1.12	1.53	1.19
L-B-1	2.32	10.2	85.8	337	59	0.82	68.9	1.25	1.51	1.19
L-B-2	2.39	10.2	86.5	356	59	0.81	70.0	1.24	1.52	1.18
L-B-3	2.28	10.2	87.3	326	59	0.82	68.0	1.28	1.54	1.22
L-D-1	2.34	10.2	89.1	356	98	0.81	79.3	1.12	1.52	1.19
L-D-2	2.26	10.2	92.1	330	98	0.82	76.8	1.20	1.58	1.25
L-D-3	2.34	10.2	92	356	98	0.81	79.2	1.16	1.57	1.22
L-F-1	2.39	12.7	103.7	369	199	0.81	91.9	1.13	1.77	1.37
L-F-2	2.24	12.7	101.2	326	199	0.82	87.7	1.15	1.73	1.38
L-F-3	2.31	12.7	105.1	347	199	0.82	89.8	1.17	1.80	1.41
L-J-1	2.36	10.2	99.3	362	103	0.81	80.8	1.23	1.70	1.31
L-J-2	2.36	10.2	100.2	362	103	0.81	80.8	1.24	1.71	1.33
L-J-3	2.43	10.2	104.1	382	103	0.81	82.2	1.27	1.78	1.36
M-A-1	1.83	10.2	131.4	394	98	0.87	114.1	1.15	1.41	1.12
M-A-2	1.79	10.2	128.7	376	98	0.88	111.8	1.15	1.38	1.11
M-A-3	1.80	10.2	132.1	382	98	0.88	112.4	1.17	1.41	1.14
M-F-1	1.77	12.7	146.1	369	189	0.88	125.3	1.17	1.56	1.27
M-F-2	1.67	12.7	135	326	189	0.89	117.6	1.15	1.45	1.23
M-F-3	1.72	12.7	144.3	347	189	0.89	121.5	1.19	1.55	1.29
M-J-1	1.76	10.2	141	362	120	0.88	114.2	1.23	1.51	1.24
M-J-2	1.74	10.2	137.2	356	120	0.88	113.1	1.21	1.47	1.21
M-J-3	1.74	10.2	135.4	356	120	0.88	113.3	1.19	1.45	1.20
S-A-1	1.13	10.2	163.3	354	98	0.99	147.8	1.10	1.21	0.90
S-A-2	1.13	10.2	161.9	360	98	0.98	149.5	1.08	1.20	0.88
S-A-3	1.16	10.2	165.4	379	98	0.98	155.1	1.07	1.22	0.88
S-B-1	1.17	10.2	156	354	56	0.98	132.4	1.18	1.19	0.89
S-B-2	1.18	10.2	160.7	360	56	0.98	133.7	1.20	1.22	0.91
S-B-3	1.14	10.2	155	335	56	0.98	126.9	1.22	1.18	0.91
S-D-1	1.13	10.2	160	354	98	0.99	147.8	1.08	1.18	0.88
S-D-2	1.13	10.2	163.1	360	98	0.98	149.5	1.09	1.21	0.89
S-D-3	1.16	10.2	166.8	379	98	0.98	155.1	1.08	1.23	0.88
S-F-1	1.13	12.7	172.9	354	189	0.99	165.1	1.05	1.28	0.95
S-F-2	1.13	12.7	179.2	360	189	0.98	167.3	1.07	1.32	0.98
S-F-3	1.13	12.7	171.1	360	189	0.98	167.3	1.02	1.26	0.93
S-J-1	1.15	10.2	180.6	369	130	0.98	159.9	1.13	1.33	0.97
S-J-2	1.13	10.2	176.7	360	130	0.98	157.9	1.12	1.31	0.96
S-J-3	1.16	10.2	182.1	379	130	0.98	162.4	1.12	1.35	0.97
Schneider 2003, L80/8 and L120/12									
21	1.21	25	401.2	589	2279	0.97	371.5	1.08	2.18	1.42

10

22	1.21	25	409.6	589	2279	0.97	371.5	1.10	2.23	1.45
25	2.77	15	169.7	589	492	0.78	132.8	1.28	2.40	1.75
26	2.77	15	165.5	589	492	0.78	132.8	1.25	2.34	1.71
27	1.52	15	372.9	903	492	0.92	318.9	1.17	1.26	1.10
28	1.52	15	373.7	903	492	0.92	318.9	1.17	1.26	1.10

1. values were calculated with measured yield strength of tests	min :	1.02	1.18	0.88
2. $c_{\varphi,in} = \infty$ for all configurations	max:	1.53	2.45	1.96
3. results compared with AISC 360-16	mean:	1.19	1.57	1.22
4. results compared with EN 1993-1-1	COV:	0.012	0.113	0.073

In order to extend the validation of the design model to all investigated connection details, a FE parametric study was carried out on 3D-models, including angle member and detailed joint configuration, with the software ABAQUS. In total, 296 numerical ultimate load calculations were conducted. 72 each for detail 1 and detail 2 and 144 for detail 3. The mesh density and element types were adopted from the optimized and calibrated FE models from Kettler et al. 2021. In the region of the joints, the angle member, the welds as well as the adjacent structure (gusset plate or girder flange) were modelled by solid elements (type C3D8R). For the inner part of the angle member, shell elements were used (type S4R), ignoring the fillets in the corner and at the leg tips. The material behaviour was assumed as linear elastic – ideal plastic ($E = 210\,000$ MPa, $\nu = 0.30$, $f_y = 235$ MPa for S235) without any safety factors.
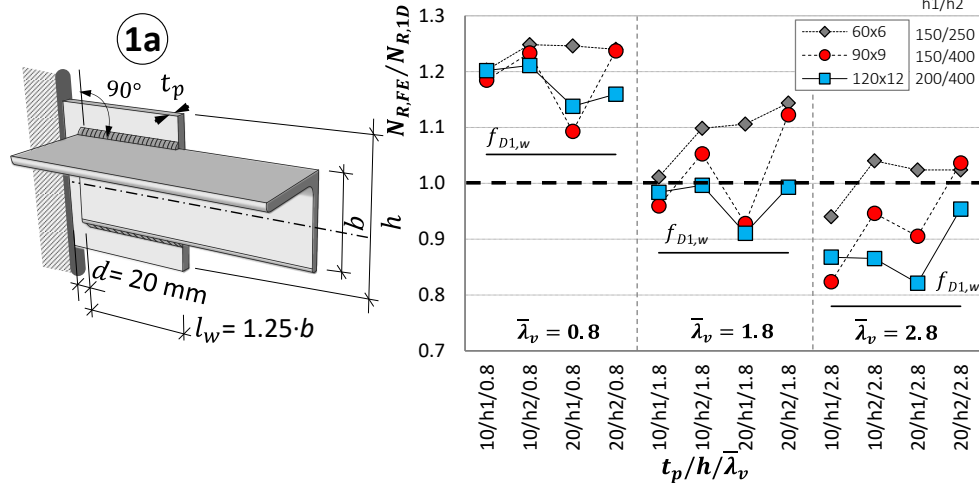

Figure 8: Comparison of design proposal with FE parametric study for detail 1a and calibration of factor $f_{D1a,w}$.

Fig.8 presents a comparison of the results of the proposed design model without calibration factor $f_{Di,w}$ (i.e. $N_{R,1D}$) with the results of the FE-model ($N_{R,FE}$) for individual member configurations (in total 36 cases) with fixed gusset plate connections (detail 1a). Three different angle members (L 60x6, L 90x9 and L 120x12) are presented, with three different relative slenderness values ($\bar{\lambda}_v = 0.8; 1.8; 2.8$, based on system length L). Different geometries of the gusset plate are studied, with variation of the thickness t_p (10 or 20 mm) and the height h (values h_1 or h_2 in Fig. 8 with 150, 200, 250 or 400 mm). The weld length was assumed with $l_w = 1.25 \cdot b$, where b is the width of the angle leg. The free length of the gusset plate was assumed as $d = 20$ mm. Based on the results in Fig. 8, and additional results for detail 1b, the calibration factor $f_{D1,w}$, already presented in Eq. (2), is suggested. The accuracy of the derived factor is verified in Table 2.

Fig. 9 and Fig. 10 present the comparison of member capacities ($N_{R,FE}/N_{R,1D}$) for detail 2a and detail 3a-1, respectively. For the latter, the gusset plate is attached to the girder web at mid-height. Again the same angle types (L 60x6, L 90x9 and L 120x12) and relative slenderness values ($\bar{\lambda}_v =$

11

0.8; 1.8; 2.8) are studied. Additionally, two very different girder types are investigated for both details (HEB 200, HEA 800 for detail 2a and HEA 600 and HEA 1000 for detail 3a-1) with two different support ratios ($L_g/h_w = 10$; 20). The angle member in compression is attached to the girder at mid-span. The horizontal deformations of the girder are prevented at the position of the angle-to-girder-connection, assuming that the angle strut is part of a lattice in the plain of the upper flange or the plain of the gusset plate for detail 2a and detail 3a-1, respectively. Based on the results in Fig. 9 and Fig. 10, the calibration factors $f_{D2,w}$ and $f_{D3,w}$, already presented in Eqs. (3) and (4), are suggested.
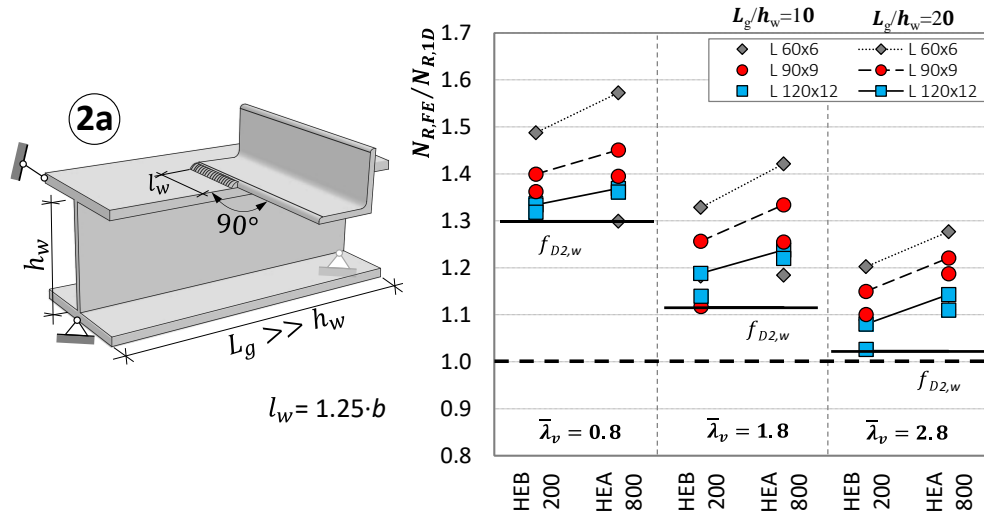

Figure 9: Comparison of design proposal with FE parametric study for detail 2a and calibration of factor $f_{D2,w}$.
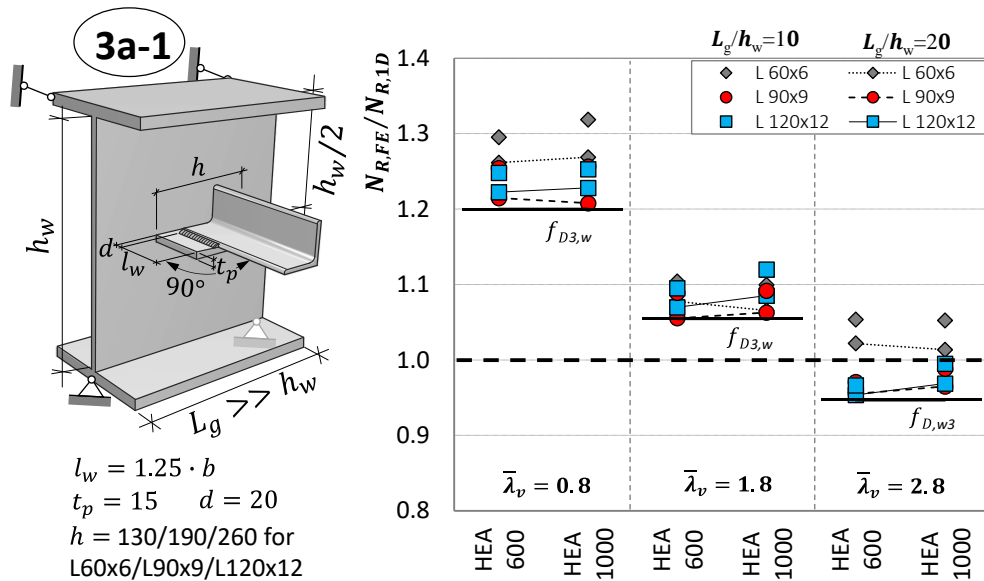

Figure 10: Comparison of design proposal with FE parametric study for detail 3a-1 and calibration of factor $f_{D3,w}$.

Table 2 summarizes the comparison of results of all conducted 296 ultimate load calculations of the FE parametric study with AISC 360, EN 1993-1-1 and the design model on basis of the ratio $N_{R,FE}/N_{R,code}$ and $N_{R,FE}/N_{R,model}$, respectively. The statistical parameters presented are the minimum value, the maximum value, the mean value and the coefficient of variation. The presented data is

based on 72 results for every line. 36 results for cases of type 'a' with the member axis perpendicular to the support or the girder and 36 results for cases of type 'b' which show an inclination of 45°. The results for detail 3-1 consider gusset plates that are attached to the girder web at mid-height (i.e. $u/h_w = 0.5$, where u is the distance from the gusset plate to the upper flange). Detail 3-2 considers cases with $u/h_w = 0.33$. The results in Table 2 verify that the proposed design model is able to accurately predict the compression strength of angle sections for the investigated welded end connection details. The model is slightly conservative throughout the whole investigated parameter range. The very small coefficients of variation clearly indicate that the model is able to accurately incorporate the effect of rotational restraints at the member's ends provided by the adjacent structure. The corresponding comparison for the current design provisions (AISC 360, EN 1993-1-1) shows significant less favourable results.

Table 2: Comparison of FE parametric study with AISC 360, EN 1993-1-1 and design model

Detail type[1]	$N_{R,FE}/N_{R,code}$ - AISC 360, E5.(a)				$N_{R,FE}/N_{R,code}$ - EN 1993-1-1				$N_{R,FE}/N_{R,model}$ - design model			
	Min	Max	Mean	COV	Min	Max	Mean	COV	Min	Max	Mean	COV
Detail 1	0.80	2.08	1.25	0.102	0.70	2.10	1.25	0.136	1.00	1.39	1.14	0.010
Detail 2	0.93	2.19	1.36	0.105	0.82	2.19	1.37	0.138	1.00	1.31	1.12	0.006
Detail 3-1	0.87	1.70	1.15	0.051	0.76	1.85	1.16	0.086	1.00	1.13	1.05	0.001
Detail 3-2	0.86	1.70	1.15	0.052	0.76	1.85	1.16	0.086	1.00	1.15	1.07	0.001

1. 72 individual cases for each detail (50% detail type a, 50% detail type b)

5. Conclusions
This paper illustrates that the compression member capacity of welded angle struts with different joint configurations (detail 1 to 3) can be calculated as for bolted angle members by means of an elastic second order analysis of the individual member that takes into account an equivalent bow imperfection and eccentricities as well as accurate rotational restraints at the member's ends. The design check is fulfilled, if the maximum direct stresses, based on the design load N_{Ed}, in the angle member are not larger than the yield strength f_y multiplied with a calibration factor $f_{Di,w}$ that is a function of the slenderness $\bar{\lambda}_v$.

Comparisons with experimental tests and with a comprehensive 3D-FE parametric study (with detailed modelling of the joint configurations) confirm that the presented design procedure for welded angle members is able to accurately incorporate the effect of rotational restraints at the member's ends provided by the adjacent structure. The proposed design model is shown to be slightly conservative throughout the whole investigated parameter range. Similar comparisons for the current code provisions of AISC 360 and EN 1993-1-1 highlight that the design specifications pragmatically take into account a certain small rotational end restraint, but that they are not capable of distinguishing between different support conditions in real structures. This can lead to unsafe as well as uneconomic compression capacity predictions.

References

ANSI. (2016). "AISC 360-16, Specification for Structural Steel Buildings." Chicago.

CEN. (2014). "EN 1993-1-1, Eurocode 3: Design of steel structures – Part 1-1: General rules and rules for buildings." Brussels.

Kettler, M., Taras, A., Unterweger, H. (2017). "Member capacity of bolted steel angles in compression: Influence of realistic end supports." *Journal of constructional steel research*, 130, 22-35.

Kettler, M., Lichtl, G., Unterweger, H. (2019). "Experimental tests on bolted steel angles in compression with varying end supports." *Journal of constructional steel research*, 155, 301-315.

Kettler M., Unterweger H., Harringer T. (2019a). „Appropriate spring stiffness models for the end supports of bolted angle compression members." *Steel Construction*, 12, No. 4, 291-298.

Kettler, M., Unterweger, H., Zauchner, P. (2021). "Design proposal for bolted angle members in compression including joint stiffness." *Journal of constructional steel research*, 184, 106778.

Sakla S.S.S. (1997). "Single-angle compression members welded by one leg to gusset plates." *PhD thesis*, University of Windsor.

Schneider R.W. (2003) „Beitrag zur Bemessung von druckbeanspruchten Einzelwinkeln unter Berücksichtigung der Anschlusseigenschaften." *PhD thesis*, RWTH Aachen, Shaker Verlag (No. 48).

Trahair N.S., Usami, T., Galambos, T.V. (1969). "Eccentrically loaded single-angle columns." *Research report No. 11*, Civil and Environmental Department, Washington University, St. Louis, MO.